Rock Mechanics and Rock Engineering (2022) 55:5535–5554
https://doi.org/10.1007/s00603-022-02948-y

ORIGINAL PAPER

Experimental Study and Soft Computing Modeling of the Unconfined Compressive Strength of Limestone Rocks Considering Dry and Saturation Conditions

Saif Alzabeebee[1] · Diyari Abdalrahman Mohammed[2] · Younis Mustafa Alshkane[2]

Received: 2 February 2022 / Accepted: 24 May 2022 / Published online: 22 June 2022
© The Author(s), under exclusive licence to Springer-Verlag GmbH Austria, part of Springer Nature 2022

Abstract

Unconfined compressive strength (UCS) of intact limestone rocks is very significant in geotechnical engineering in order to design structures that are currently being built on/in these rocks safely and economically. Obtaining core samples and testing them in laboratory according to the available standards is very expensive and time consuming. Therefore, developing novel models to predict the UCS of limestone rocks using physical properties and non-destructive tests is crucially needed. Hence, the research in this paper has been conducted to address this aim. 104 samples of intact limestone rocks have been collected from two provinces in north of Iraq (Sulaymaniyah and Mosul). The UCS, Schmidt hammer rebound number, ultrasonic pulse velocity, dry density, saturated density, and porosity have been obtained for these samples. One-dimensional regression analysis and advanced evolutionary polynomial regression (EPR-MOGA) analysis have been conducted using the obtained results. It was found that the EPR-MOGA analysis showed improved prediction performance and generally the prediction accuracy increases as the number of the variables increases. The models developed using EPR-MOGA have been compared to a simple regression equation proposed in the literature for north of Iraq limestone rocks, where it was found that the new models outperform the available correlation. The proposed models could be of significant help to practitioners when the compression testing machine is not available or when it is difficult to obtain intact samples with the appropriate length to diameter ratio. The proposed models could also serve as a tool to do independent quality control check of UCS laboratory results.

Highlights

- Limestone rock samples have been collected from different location in north of Iraq.
- Dry and saturated limestone rock samples have been tested in the laboratory.
- Nondestructive and unconfined compressive strength tests have been conducted on the samples.
- UCS cannot be accuracy estimate using one-dimensional regression analysis.
- Novel models have been developed to predict the UCS from non-destructive tests using EPR-MOGA.

Keywords Unconfined compressive strength · Limestone rock · EPR-MOGA · Soft computing · Schmidt hammer · And ultrasonic pulse velocity

✉ Saif Alzabeebee
Saif.Alzabeebee@gmail.com; Saif.Alzabeebee@qu.edu.iq

Diyari Abdalrahman Mohammed
diyari.mohammed@univsul.edu.iq

Younis Mustafa Alshkane
younis.ali@univsul.edu.iq

[1] Department of Roads and Transport Engineering, University of Al-Qadisiyah, Al-Qadisiyah, Iraq

[2] Department of Civil Engineering, College of Engineering, University of Sulaimani, Sulaimani, Kurdistan Region, Iraq

1 Introduction

Limestones are widely spread in mountain areas in north of Iraq governorates in many formulations (Numan et al. 1998; Aziz and Baban 2005; Mirza et al. 2016; Sissakian et al. 2021). There are many structures that are currently being constructed on/in these rocks. Robust and safe design of these structures require an accurate determination of the unconfined compressive strength of these rocks (Sabatakakis

et al. 2008; Jabbar 2011; Singh et al. 2012; Mishra and Basu 2013; Yurdakul and Akdas 2013; Barone et al. 2015; Kurtuluş et al. 2016; Daoud et al. 2017, 2018; Wang and Wan 2019). However, obtaining samples and testing them in laboratory environment in accordance with the available standards (ASTM-D7012 2014; ISRM 1981; Cargill and Shakoor 1990; Kahraman 2001) is very expensive and time consuming (Feng and Jimenez 2014). It also needs expert staff that is not always available. Furthermore, in some rock masses, drilling process is very difficult because of poor quality of rock formation. Hence, it is crucial to have robust models that can be used to predict the UCS using properties that can be easily obtained from field and/or laboratory tests.

On the other hand, there are very limited studies that attempted to study the effect of saturation of limestone rocks on the mobilized UCS (Sachpazis 2004; Vásárhelyi 2005; Cherblanc et al. 2016), although the lime is sensitive to the presence of water. In addition, there is no robust correlation that enables predicting the UCS for the case of saturated limestone rocks. More importantly, most of the available correlations proposed in previous studies for the case of limestone rocks have employed simple one-dimensional regression analysis or multiple regression analysis in the development of the correlations (Deer and Miller 1966; Katz et al. 2000; Kahraman 2001; Azimian 2017; Hebib et al. 2017; Kong and Shang 2018; Mohammed et al. 2020). These available correlations are shown in Table 1. In addition, there have been limited attempts to utilized advanced techniques to provide explicit models to predict the UCS, where most of the studies used artificial intelligence-based techniques with no explicit models being proposed to predict the UCS (Baykasoğlu et al. 2008; Monjezi et al. 2012; Yurdakul and Akdas 2013; Momeni et al. 2015). Hence, it is necessary to utilize robust soft computing techniques to provide models to estimate the UCS of limestone rocks from simple and inexpensive tests and in accuracy better than the correlations that have been developed using simple regression analysis, bearing in mind that there have been much evidence in the literature on the superiority of soft computing techniques over the classical regression analysis (Ozer et al. 2008; Shahnazari and Tutunchian 2012; Alzabeebee and Chapman 2020). Therefore, to address these gaps in knowledge, this study aims to focus on the following:

1. Conduct experimental program to investigate the effect of water saturated on the UCS of limestone rocks.
2. Investigate the relationship between the Schmidt hummer rebound number and the UCS, and ultrasonic pulse velocity and the UCS for dry and saturated limestone rocks.
3. Develop novel models to predict the UCS of dry and saturated limestone rocks using simple properties of rocks that can be easily obtained from laboratory and/or field tests using advanced soft computing techniques.

2 Methodology of the Study

The methodology of the work involves three parts. The first part involves collecting limestone rock samples and testing these samples in the laboratory. The second part involves applying robust soft computing algorithm to predict the UCS of limestone rock from simple indices. The third part involves the use of statistical-based performance indicators to examine the quality of the proposed models in comparison to the recent correlation proposed to predict the UCS for limestone rocks, which is the correlation of Mohammed et al. (2020).

Table 1 Available equations to predict the UCS for limestone rocks

References	Equation
Kahraman (2001)	$UCS = 9.95V_p^{1.21}$
Deer and Miller (1966)	$UCS = 1246RL - 34890$
Katz et al. (2000)	$UCS = 2.208e^{0.067RL}$
Kahraman (2001)	$UCS = 6.97e^{0.014RL}$
Minaeian and Ahangari (2013)	$UCS = 0.056V_p + 0.315RL - 0.46$
Azimian (2017)	$UCS = 1.530RL + 0.11V_p - 24.673$
Hebib et al. (2017)	$UCS = 2.855e^{0.0632RL}$
Kong and Shang (2018)	$UCS = 0.30RL^{1.43}$
Mohammed et al. (2020)	$UCS = 58.991 \times \exp^{(0.032 \times RL)} - 74.128$

UCS is the unconfined compressive strength, V_p is the ultrasonic pulse velocity of the rock, and RL is the Schmidt hammer rebound number

2.1 Experimental Program

2.1.1 Study Areas

The rocks samples employed in this research have been collected from Sulaymaniyah and Mosul provinces. The location of these governorates is shown in Fig. 1. Sulaymaniyah province is located in the north-east of Iraq and Mosul province is located in the northern part of Iraq. The samples have been collected from three different locations in Sulaymaniyah province and two different locations in Mosul province. The coordinates of these locations are presented in Table 2. In total, 104 core samples of limestone have been collected from the aforementioned provinces. The diameter of the collected limestone core samples is equal to 54.7 mm as recommended in the ISRM (1981). In addition, the core samples have been taken from different layers using core drilling machine to obtain samples with different strength and ensure accurate representation of the limestone's rocks of the sites of the study. These samples have been used to perform physical and mechanical tests as will be explained in the following subsections. It is worthy to add that dry and saturated conditions have been used in this study to understand how the saturation influences the unconfined compression strength and also to develop models for both conditions. Hence, for each site and each layer two core samples have been obtained. One is used in the dry scenario, while the other is used in the saturated scenario. However, there have been some difficulties in limited conditions, where it was only possible to obtain one sample. Therefore, the number of samples for dry and saturated conditions are equal to 53 and 51, respectively.

Fig. 1 The location of current study (Google 2021)

2.1.2 Sample Preparation

ASTM standard and suggested methods by ISRM are used for sample preparation and testing. Rock trimming machine, shown in Fig. 2a, has been used to cut the samples. Core size diameter of 54.7 mm with length to diameter ratio of 2:1 has been prepared to take the samples. In addition, tests have been carried out to obtain the porosity (η), dry density (ρ_d) and saturated density (ρ_{sat}) of the obtained samples, where the tests have been conducted in accordance with the ISRM (1981). In addition, the samples to find the ultrasonic pulse velocity (V_p) and the unconfined compressive strength (UCS) have been prepared according to the ISRM (1981) and the ASTM-D7012 (2014), respectively. The sample ends were further smoothened using a surface grinding machine. A core size diameter of 54.7 mm with length of 100 mm was utilized for Schmidt hammer rebound number (RL) test in accordance with the ISRM (1981). In addition, it is worthy to state that the prepared samples were divided into two groups; the first group of samples was tested in dry case whereas the other group was tested in saturated case. The samples were saturated using the saturation machine shown in Fig. 2b.

2.1.3 Uniaxial Compressive Strength Test

Uniaxial compressive strength (UCS) has been performed according to the ASTM D7012-14e1 (2014) for the prepared limestone samples with core size diameter of 54.7 mm and a length to diameter ratio of 2.0. A stress rate of 0.5 MPa/s

Table 2 Sampling locations, formations, coordinates, and limestone types

Cities	Formations	Locations	Longitude	Latitude	Number of drilled samples
Sulaymaniyah	Kometan	Qlyasan	35.600577	45.376724	20
	Pila Spy	Qaradax	35.366317	45.476043	27
	Sinjar	Tasluja	35.590784	45.227209	26
Mosul	Lower Fars	Ayn al-Jahesh	35.996230	42.827273	24
	Lower Fars	Al-Shora	35.997092	43.225531	16

(a) Rock trimming machine **(b)** Saturation machine

Fig. 2 **a** Rock trimming machine; **b** saturation machine (Mohammed et al. 2020)

has been used in the test. This stress rate has been selected according to the ISRM (1981). This stress rate also satisfies the requirements of the ASTM D7012-14e1 (2014) as the test time ranges between 2 and 15 min. UCS test performed using the compression testing machine shown in Fig. 3 which was manufactured by Control Company with capacity of 3000 kN.

2.1.4 Schmidt Hammer Test (L-type)

L-type Schmidt hammer rebound number (RL) has been performed using core size diameter of 54.7 mm with length of 100 mm. The samples ends have been smoothed according to requirement of the ISRM (1981). Additionally, the procedure of the test was performed according to the ISRM (1981) with the direction of the hammer perpendicular to the tested surface. L-type hammer (energy of 0.735 N.m) with a steel base of a minimum weight of 20 kg has been used as shown in Fig. 4.

2.1.5 Ultrasonic Pulse Velocity Test

The procedure of direct transmission pulse velocity test has been conducted based on the ISRM (1981) by using core size diameter of 54.7 mm with a length to diameter ratio of 2. Ultrasonic testing device (Fig. 5) consists of ultrasonic tester 58E48, one transmitter, one receiver head, 54 kHz type, two connecting cables, and one calibration.

2.1.6 Porosity and Density Properties

The tests to obtain the apparent porosity (η), dry unit weight (ρ_d) and saturated unit weight (ρ_{sat}) properties have been conducted based on the ISRM (1981) using saturation and caliper techniques. In addition, oven with capacity over 105 ºC, sensitive balance and saturation machine have been used to find η, γ_d and γ_{sat}.

Fig. 3 Compression testing machine (Mohammed et al. 2020)

2.2 Soft Computing Algorithm

The multi-objective evolutionary polynomial regression analysis (EPR-MOGA) has been employed in this study to propose the new models. The algorithm of the EPR-MOGA are well known and its robustness has been proved by many studies in the field of geotechnical engineering (Alzabeebee et al. 2021a, b). It employs the regression analysis methodology with the search being aid using an optimized genetic algorithm methodology. The desirable output models, the range of the exponents, and the number of terms for the correlation are all defined in trial-and-error stages with the aid of the experience of the user.

Fig. 4 Hammer test apparatus (L-type) (Mohammed et al. 2020)

Fig. 5 Ultrasonic testing device

The technique of the EPR-MOGA is primarily based on developing candidate mathematical models that correlate the input and output data with the aid of an evolutionary technique that considers the benefits of genetic algorithm. The candidate mathematical models develop in complexity in the evolutionary process based on the number of terms and range of exponents proposed in the initial analysis stage. Initially, the candidate mathematical models are developed based on Eq. 1 (Giustolisi and Savic 2006, 2009).

$$Y = \sum_{j=1}^{m} F\left(\mathbf{X}, f(\mathbf{X}), a_j\right) + a_0, \tag{1}$$

where Y is the predicted value from the EPR model (UCS in this paper); a_j is the constant of the model; F is a proposed function in the initial stage, which evolves in the process of the evolutionary computing, $\mathbf{X}$ is the matrix of the input variables; $f(\mathbf{X})$ is the type of proposed function as proposed in the initial stage; and m is the number of terms of the proposed model.

This equation is expanded based on the proposed initial form of the model (polynomial, logarithmic, exponential, tangent hyperbolic, or secant hyperbolic). Then the system is solved using least square method and employing genetic algorithm with objectives criteria to control the fitness of the model and ensure the accuracy is achieved. Also, an iterative process is conducted to reach the highest possible accuracy. Figure 6 shows the flow chart of the EPR-MOGA algorithm. Also, additional details on the EPR-MOGA could be found in many previous studies (e.g., Giustolisi and Savic 2006, 2009; Alzabeebee and Chapman 2020; Alzabeebee 2020).

2.3 Accuracy Examination

The accuracy of the developed models in this paper and the correlation proposed by Mohammed et al. (2020) has been examined using two stages. In the first stage, the statistical performance has been examined by calculating the mean absolute error (MAE), mean, and coefficient of correlation (R). Equations 2–4 have been employed in the calculation of the aforementioned indictors (Beiki et al. 2013; Zhang and Goh 2016; Ebdali et al. 2020; Miah et al. 2020; Zhang et al. 2020; Mahmoodzadeh et al. 2021, 2022). The second stage involved examining the cumulative error by obtaining and plotting the relationship between the error level and the cumulative frequency of the error. This step has been employed because the MAE, mean, and R do not provide a thorough insight into the prediction accuracy as discussed by Alzabeebee et al. (2021a, b).

$$\mathrm{MAE} = \frac{1}{n}\sum_{1}^{n}\left|\mathrm{UCS}_{(p)} - \mathrm{UCS}_{(m)}\right|, \tag{2}$$

$$\mathrm{Mean} = \frac{1}{n}\sum_{1}^{n}\left(\frac{\mathrm{UCS}_{(p)}}{\mathrm{UCS}_{(m)}}\right), \tag{3}$$

$$R = \frac{\sum_{i=1}^{n}\left(\mathrm{UCS}_{(p)} - \mathrm{UCS}_{(p)_{\mathrm{average}}}\right)\left(\mathrm{UCS}_{(m)} - \mathrm{UCS}_{(m)_{\mathrm{average}}}\right)}{\sqrt{\sum_{i=1}^{n}\left(\mathrm{UCS}_{(p)} - \mathrm{UCS}_{(p)_{\mathrm{average}}}\right)^2 \sum_{i=1}^{n}\left(\mathrm{UCS}_{(m)} - \mathrm{UCS}_{(m)_{\mathrm{average}}}\right)^2}}, \tag{4}$$

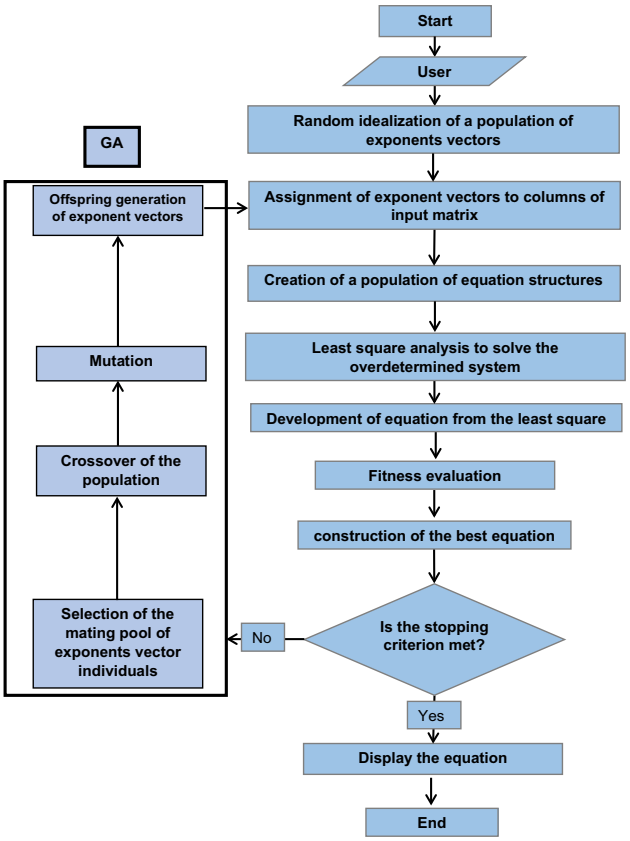

Fig. 6 The steps of the EPR-MOGA analysis (Ahangar-Asr et al. 2014; Alzabeebee 2020)

where $UCS_{(p)}$ is the predicted unconfined compressive strength, $UCS_{(m)}$ is the measured unconfined compressive strength, and n is the number of data points employed in the analysis.

3 Discussion of the Results and New Models' Development for the Dry Case

3.1 Results of the Laboratory Tests

The results obtained from the laboratory program have been first employed in a simple one-dimensional regression analysis to investigate the effect of each of the determined properties (RL, V_p, η, ρ_d and ρ_{sat}) on the unconfined compressive strength of rock (UCS). Thus, the binary relationship between the UCS and RL, V_p, η, ρ_d and ρ_{sat} are plotted in Fig. 7a-e.

It is evident from Fig. 7a, b that increasing the UCS rises as the RL and V_p increases. In addition, the figures clearly show a good correlation between the UCS and the RL, where the coefficient of correlation is equal to 0.79; while lower coefficient of correlation is obtained between the UCS and the V_p ($R = 0.69$). Figure 7c shows that increasing the porosity of the rock generally reduces the mobilized UCS; however, the correlation is not completely clear for the dry samples as the achieved correlation is poor compared to the aforementioned correlations, where the R is equal to 0.61. Finally, Fig. 7d, e show an increase in the UCS as the dry and saturated unit weight of the rock increase with a coefficient of correlation of 0.69 for the UCS–ρ_d relationship, and UCS–ρ_{sat} relationship. Importantly, it should be stated that although the trend line obtained from the binary correlations is reasonable and justifiable, it is also evident that the defined trend is not perfect which means that the UCS cannot be predicted using only single property from the aforementioned rock properties. Thus, the combined contribution of these parameters to the UCS will be examined in the next subsection using the EPR-MOGA.

Finally, to summarize the laboratory program output, Table 3 presents the statistics of the obtained results for the dry case. In addition, all of the obtained results are presented in Appendix A in Table 11 to enable using these results in future studies.

3.2 Development of the New Models

The database developed from the laboratory program have been divided into two parts. The first part of the data controls the development of the new models (training data), while the other part examines the accuracy of the model in predicting unseen results (testing data). Random function available in excel is used to ensure random separation of data. However, special attention is paid in the division of the data so that the range of the testing data be within the range of the training data to avoid extrapolation of predictions (Alzabeebee 2019). Tables 4 and 5 present the statistics of the training and testing data, respectively, where it is clear that the aforementioned condition is achieved before using the data in the analysis.

The datasets have been then used to develop new hybrid models with the aid of the EPR-MOGA algorithm. Attempts have been made to develop different hybrid models using different independent parameters to investigate the sensitivity of the predicted UCS to the intercorrelation between the independent variables (RL, V_p, η, ρ_d and ρ_{sat}). For each attempt several trials have been made by changing the general form of the model, number of terms of the model and range of the exponents to be used in the search iterations. Figure 8 presents a simplified flowchart of the methodology adopted to reach the most accurate model.

Consequently, five hybrid models have been developed, where:

- Hybrid model 1 correlates the UCS with the RL and V_p.
- Hybrid model 2 links the UCS with the RL, V_p, and ρ_d.

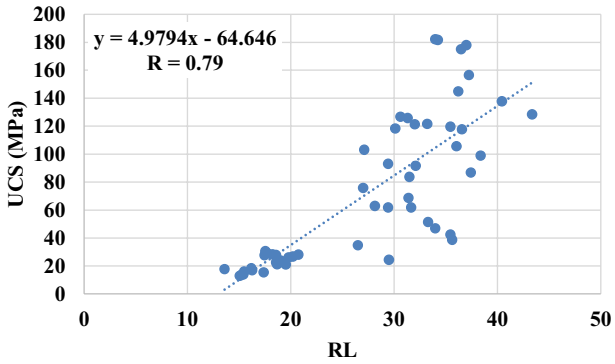

(a) UCS and RL relationship

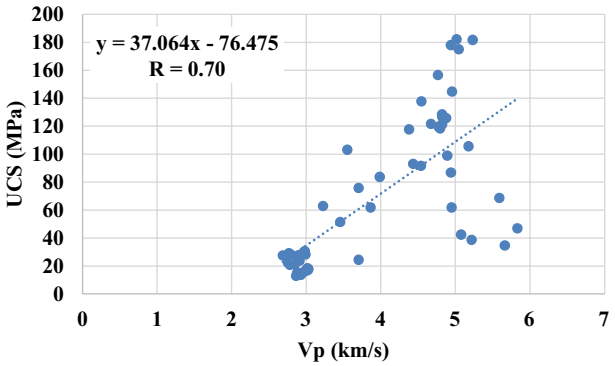

(b) UCS and Vp relationship

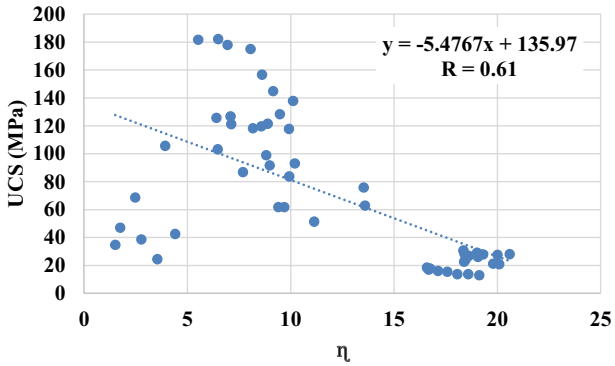

(c) UCS and η relationship

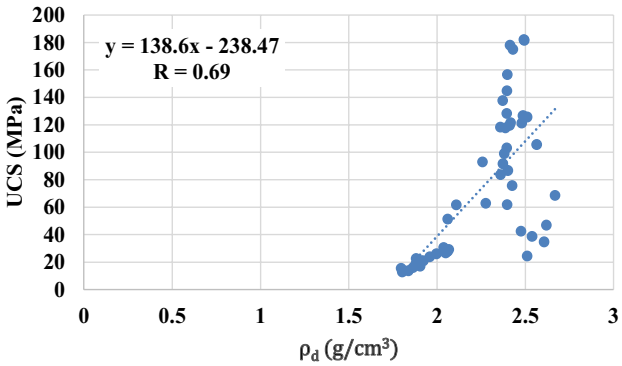

(d) UCS and ρ_d relationship

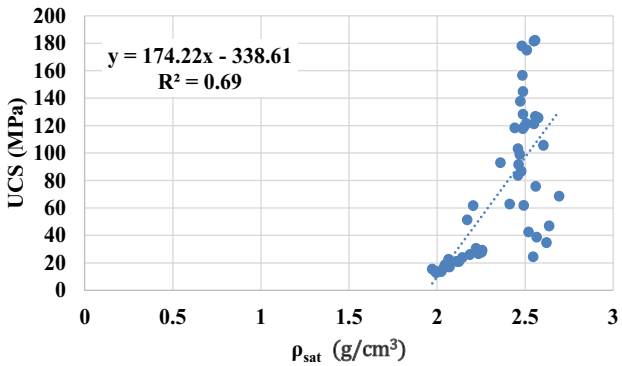

(e) UCS and ρ_{sat} relationship

Fig. 7 Binary relationship between the unconfined compressive strength and other properties of rock for the dry samples

Table 3 Statistics of the obtained results for the dry case

Statistical measure	UCS (MPa)	RL	V_p	η	ρ_d (gm/cm^3)	ρ_{sat} (gm/cm^3)
Minimum	12.97	13.59	2.69	1.51	1.80	1.97
Maximum	182.15	43.35	5.83	20.60	2.67	2.69
Mean	71.81	27.40	4.00	11.72	2.24	2.36
Standard deviation	52.81	8.45	1.01	5.91	0.26	0.21

Table 4 Statistics of the training data

Statistical measure	UCS (MPa)	RL	V_p	η	ρ_d	ρ_{sat}
Minimum	12.97	13.59	2.69	1.51	1.80	1.97
Maximum	182.15	43.35	5.83	20.60	2.67	2.69
Mean	73.00	28.08	4.09	11.21	2.27	2.38
Standard deviation	50.97	8.20	1.01	5.97	0.25	0.20

Table 5 Statistics of the testing data

Statistical measure	UCS (MPa)	RL	V_p	η	ρ_d	ρ_{sat}
Minimum	15.40	2.77	5.52	1.81	1.99	13.81
Maximum	40.42	5.23	19.80	2.49	2.56	181.64
Mean	24.82	3.66	13.65	2.13	2.26	67.26
Standard deviation	9.28	0.97	5.48	0.27	0.23	61.82

- Hybrid model 3 employs the RL, V_p, and ρ_{sat} to estimate the UCS.
- Hybrid model 4 examines the accuracy of predicting the UCS as a function of the RL, V_p, and η.
- Hybrid model 5 correlates the UCS with the RL, V_p, η, ρ_d and ρ_{sat}.

After many trials to find the most suitable models following the methodology discussed in previous publications (Alzabeebee and Chapman, 2020), the best hybrid models found using the EPR-MOGA analysis are listed in Table 6. The following subsection discusses the accuracy of the developed models.

3.3 Verification of the Developed Models

In this section, the performance of the developed models is compared to the performance of the correlation proposed by Mohammed et al. (2020) using the methodology of accuracy examination discussed in Sect. 2.3. It is worthy to state that only the correlation proposed by Mohammed et al. (2020) has been employed in the comparisons because this correlation has been specifically proposed for limestone rocks in North of Iraq. However, it is based on simple one-dimensional regression analysis. Also, Mohammed et al. (2020) already showed that all of the available correlations provide poor prediction to the UCS for limestone rocks in north of Iraq. Hence, the authors did not include the other correlations for the sake of briefing and as it is already known that these correlations provide poor predictions.

Figure 9a–f compares the relationship of the obtained-measured UCS using the developed models and the correlation proposed by Mohammed et al. (2020) with the line of perfect fit for training and testing data. The figures show some scatter for the prediction of the developed models away from the perfect fit line for some cases. However, the accuracy of the prediction of the developed hybrid models is better than the correlation proposed by Mohammed et al. (2020). Figure 10a–d shows the obtained values of the MAE, Mean, and R for the developed models and the correlation of Mohammed et al. (2020). Figure 10a shows that the MAE obtained for the training and testing datasets is on the same range for all of the developed hybrid models indicating that the new models can predict unseen results. In addition, the figure also shows that hybrid models 4 and 5 scored better results for the MAE compared to hybrid models 1–3 and Mohammed et al. (2020) correlation. Figure 10b shows that all of the models scored mean with the same range for both training and testing data, indicating again excellent capabilities of the developed models to predict unseen data. In addition, it is clear from Fig. 10b that hybrid models 4 and 5 scored better mean for the training data. In addition, it is also obvious from Fig. 10b that all of the models scored better mean than the correlation of Mohammed et al. (2020). Figure 10c shows the obtained coefficient of correlation, where it is obvious from the figure that hybrid models 4 and 5 scored better coefficient of correlation compared to the other models and the correlation of Mohammed et al. (2020). Also, Fig. 10c gives similar observations to those noticed from Fig. 10a, b, where all of the models scored better performances than the correlation of Mohammed et al. (2020). It is worthy to state that it was expected that the new models score better performance than Mohammed et al. (2020) correlation because this correlation has been developed using only the Schmidt hammer results and using simple regression analysis, while the models developed in this study consider more than one parameter of the rock and have been developed using more advanced technique that allows the selection of the parameters of the model based on genetic algorithm.

Finally, Fig. 11 presents the relationship between the cumulative frequency and the error level for hybrid models 1–5 and Mohammed et al. (2020) correlation. The figure provides similar observation to that concluded from Fig. 10,

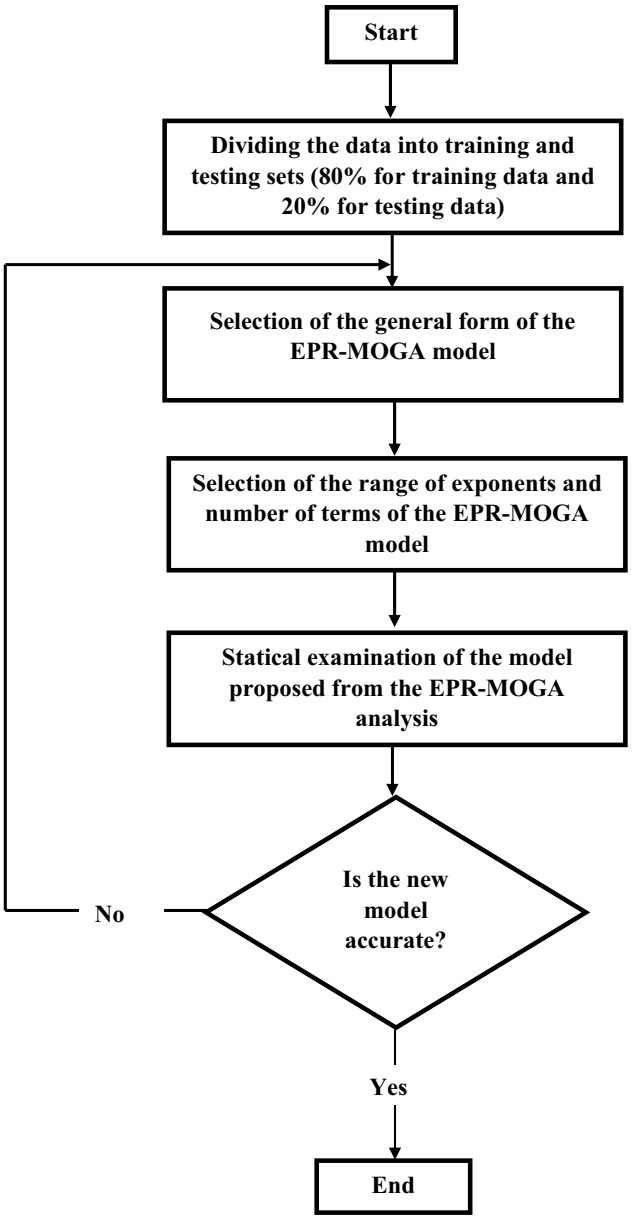

Fig. 8 Simplified flow chart of the adopted methodology to reach the highest accuracy for the EPR-MOGA models

where it is clear that hybrid model 5 scored lower error with higher frequency compared to other proposed hybrid models and also with the correlation of Mohammed et al. (2020). In addition, hybrid model 1 show better performance than hybrid models 2–4 for error level of 18–26%. However, the figure shows that the new models achieved lower error than the correlation of Mohammed et al. (2020). To conclude, it is evident that using higher number of variables enhance the prediction accuracy of the UCS for the dry condition.

Table 6 The hybrid models developed for the dry case

Correlation name	Mathematical formulation	Parameters employed in development of the hybrid model
Hybrid model 1	$UCS = -256.06 \times \sqrt{V_p} + 1.72 \times RL^{1.5} \times V_p^{1.5} - 0.563 \times RL^{1.5} \times V_p^{2.0} - 0.603 \times RL^{2.0} + 371.51$	Schmidt hummer rebound and ultrasonic
Hybrid model 2	$UCS = -4.21 \times RL^{1.5} \times V_p^2 + 5.52 \times RL^{1.5} \times V_p^2 \times \sqrt{\rho_d} - 1.8 \times RL^{1.5} \times V_p^2 \times \rho_d + 34.8$	Schmidt hummer rebound, ultrasonic and dry density
Hybrid model 3	$UCS = -0.42 \times \sqrt{RL} \times V_p^2 \times \rho_{sat}^{1.5} + 4.71 \times RL \times \rho_{sat}^2 - 3.13 \times RL^{1.5} \times V_p \times \rho_{sat}^{1.5} + 3.96 \times RL^{1.5} \times V_p^{1.5} \times \rho_{sat} - 1.31 \times RL^{1.5} \times V_p^{1.5} \times \sqrt{\rho_{sat}} - 116.05$	Schmidt hummer rebound, ultrasonic and saturated density
Hybrid model 4	$UCS = -1.91 \times V_p^2 \times \eta + 1.95 \times RL \times V_p \times \sqrt{\eta} - 2.48 \times RL^{1.5} - 0.00015 \times RL^2 \times V_p \times \eta^2 + 121.08$	Schmidt hummer rebound, ultrasonic and porosity
Hybrid model 5	$UCS = -0.156 \times V_p^2 \times \eta \times \gamma_d^{1.5} \times \sqrt{\rho_{sat}} + 0.156 \times \sqrt{RL} \times V_p^2 \times \sqrt{\eta} \times \rho_d^2 \times \sqrt{\rho_{sat}} - 0.332 \times RL \times V_p^{1.5} \times \rho_{sat}$	Schmidt hummer rebound, ultrasonic, porosity, saturated density, and dry density

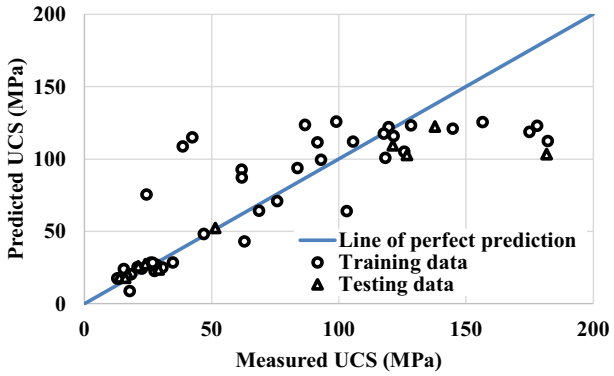

(a) Hybrid model 1

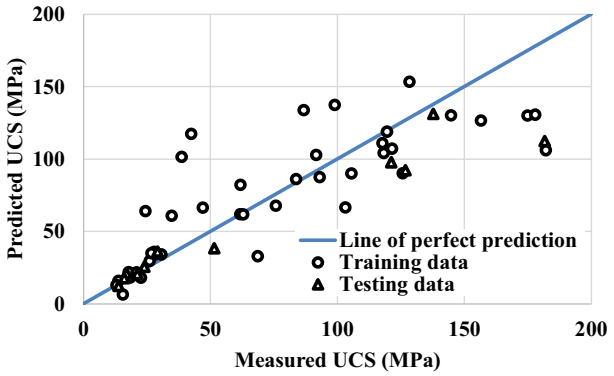

(b) Hybrid model 2

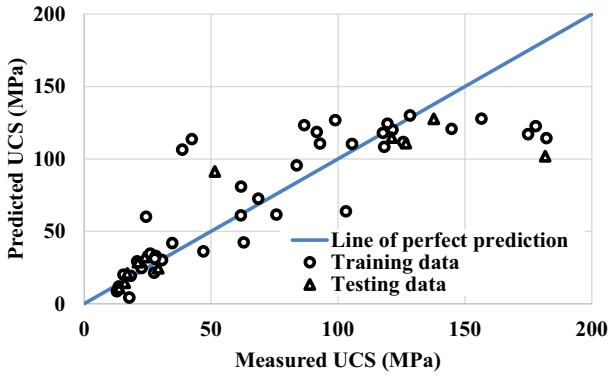

(c) Hybrid model 3

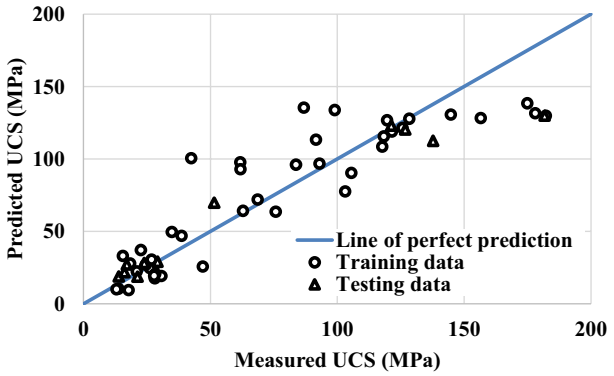

(d) Hybrid model 4

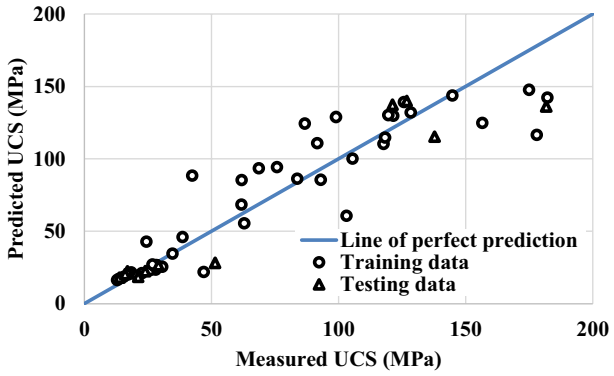

(e) Hybrid model 5

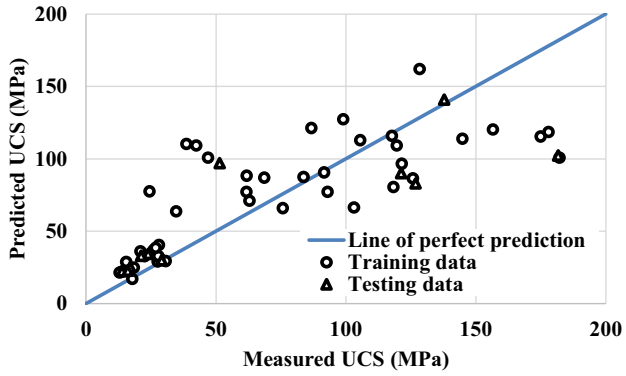

(f) Mohammed et al. (2020)

Fig. 9 Comparison of the relationship of the obtained-measured UCS with the line of perfect fit for the case of dry samples for the proposed models and the correlation of Mohammed et al. (2020)

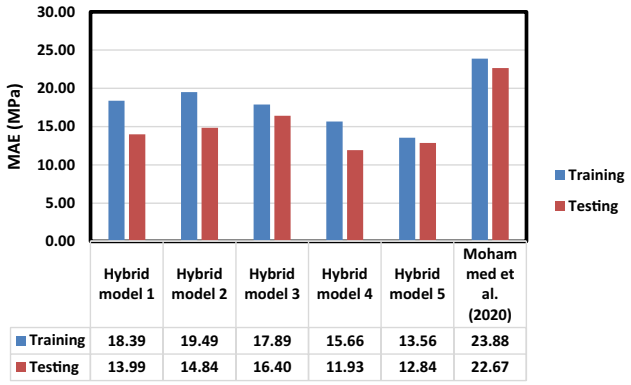

	Hybrid model 1	Hybrid model 2	Hybrid model 3	Hybrid model 4	Hybrid model 5	Mohammed et al. (2020)
Training	18.39	19.49	17.89	15.66	13.56	23.88
Testing	13.99	14.84	16.40	11.93	12.84	22.67

(a) Mean absolute error (MAE)

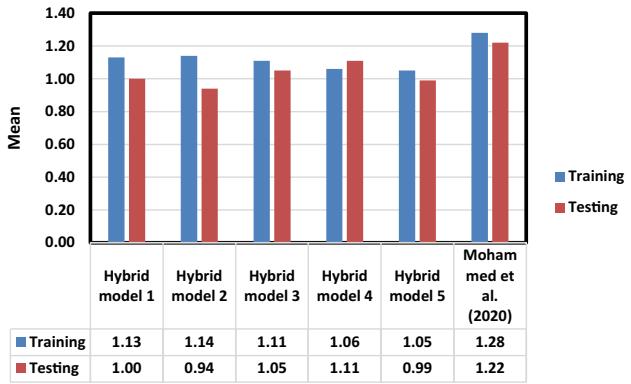

	Hybrid model 1	Hybrid model 2	Hybrid model 3	Hybrid model 4	Hybrid model 5	Mohammed et al. (2020)
Training	1.13	1.14	1.11	1.06	1.05	1.28
Testing	1.00	0.94	1.05	1.11	0.99	1.22

(b) Mean

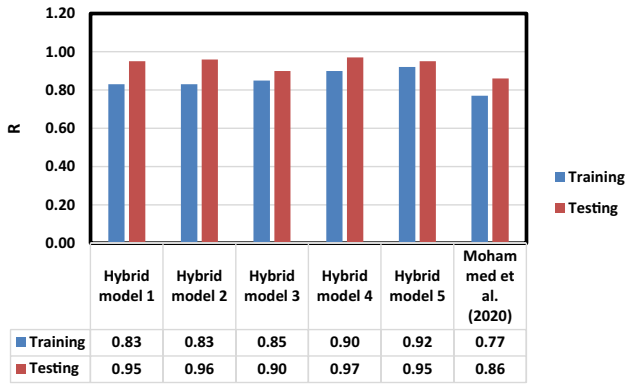

	Hybrid model 1	Hybrid model 2	Hybrid model 3	Hybrid model 4	Hybrid model 5	Mohammed et al. (2020)
Training	0.83	0.83	0.85	0.90	0.92	0.77
Testing	0.95	0.96	0.90	0.97	0.95	0.86

(c) Coefficient of correlation (R)

Fig. 10 Statistical performance of the new hybrid models and Mohammed et al. (2020) correlation

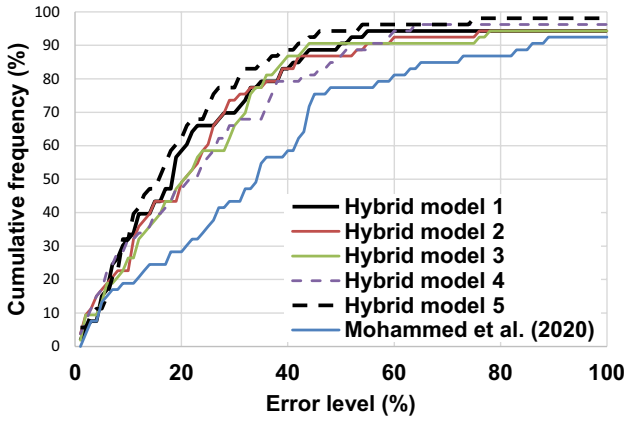

Fig. 11 Relationship between the cumulative frequency and the error level for hybrid models 1–5 and Mohmmed et al. (2020) correlation

4 Discussion of the Results and New Models' Development for the Saturated Case

4.1 Results of the Laboratory Tests

Similar to the dry case, Fig. 12a–e presents the binary correlations between the UCS and the RL, V_p, η, ρ_d and ρ_{sat}. The coefficient of correlation for each case is also presented in Fig. 12a–e. Figure 12a, b clearly show that the UCS generally rises as the RL and V_p increase. In addition, both figures show that there is a reasonable correlation between the UCS and RL; and UCS and V_p justified by the relatively high value achieved for the coefficient of correlation for both correlations (0.82 for the UCS–RL relationship and 0.81 for the UCS–V_p relationships). Figure 12c shows a general tendency for the UCS to decrease as the porosity rises, this obtained response is reasonable as the strength decreases when the volume of voids increases with the total volume being constant. The increase of the volume of voids weakens the structure of the rock and thus, reduces the ability of the rock to sustain loads. Figure 12c also shows that there is generally a reasonable relationship between the UCS and porosity, where the obtained coefficient of correlation is equal to 0.69.

Figures 12d, e show a general increase in the UCS as the dry and saturated unit weight rises; this response is also reasonable as increasing the unit weight of the rock means that the percentage of the solid parts to the voids rises, which will in turn enhance the UCS. These Fig. 5d, e also show a good correlation between the UCS and the aforementioned parameters as the coefficient of correlation scored for both relationships is equal to 0.73 and 0.71, respectively. Finally, the maximum, minimum, mean, and standard deviation of the obtained results are tabulated in Table 7 to provide better read on the ranges for the obtained results. In addition, all of the obtained results are presented in Appendix A in Table 12. Furthermore, the following section will continue on the use of these results to enhance predictions of the unconfined compressive strength.

4.2 Development of the New Models

Following the same methodology discussed in Sect. 3.1 and Fig. 8, the database initiated using the laboratory results for the saturated scenario have been divided into two subgroups

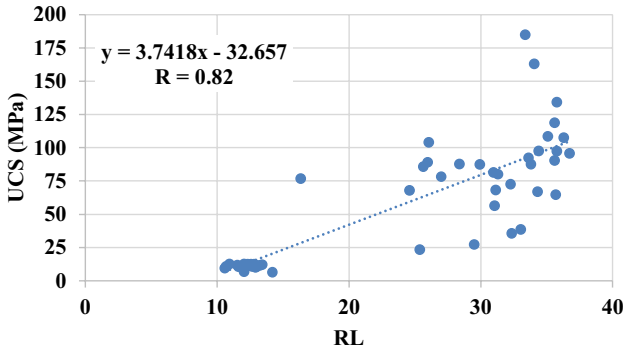

(a) UCS and RL relationship

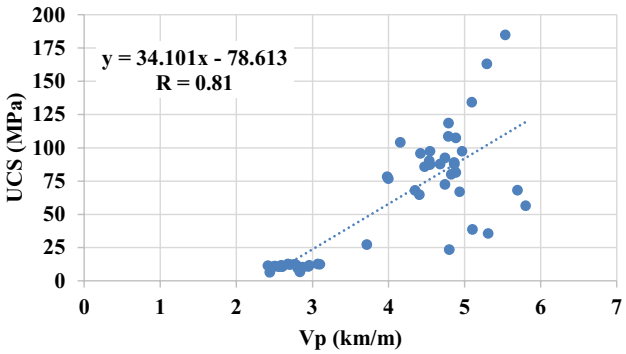

(b) UCS and Vp relationship

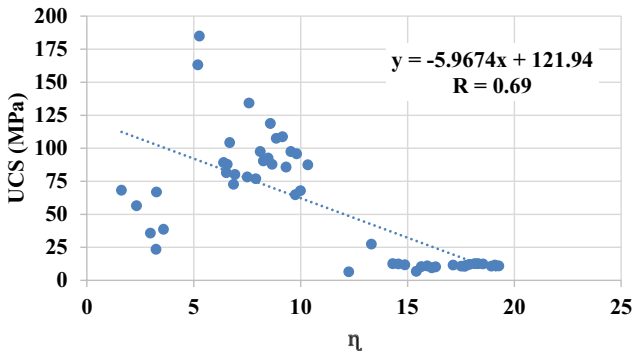

(c) UCS and η relationship

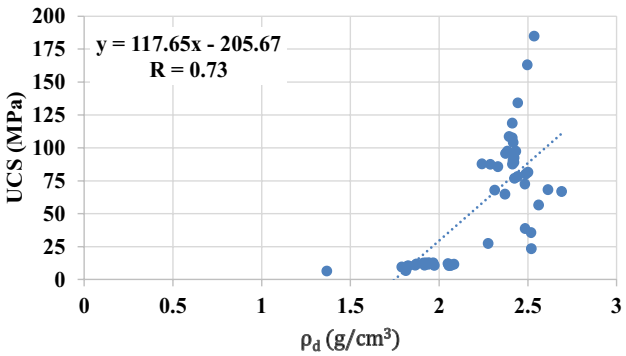

(d) UCS and ρ_d relationship

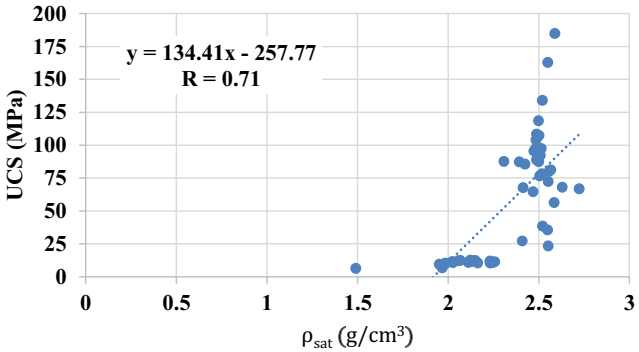

(e) UCS and ρ_{sat} relationship

Fig. 12 Binary relationship between the unconfined compressive strength and other properties of rock for the saturated samples

Table 7 Statistics of the obtained results for the saturated case

Statistical measure	UCS (MPa)	RL	V_p	η	ρ_d	ρ_{sat}
Minimum	6.45	10.58	2.41	1.62	1.37	1.49
Maximum	184.87	36.72	5.80	19.27	2.69	2.72
Mean	56.63	23.86	3.97	10.94	2.23	2.34
Standard deviation	45.73	10.05	1.08	5.31	0.29	0.24

Table 8 Statistics of the training data for the results of the saturated samples

Statistical measure	UCS (MPa)	RL	V_p	η	ρ_d	ρ_{sat}
Minimum	6.45	10.58	2.41	1.62	1.37	1.49
Maximum	184.87	36.72	5.80	19.27	2.69	2.72
Mean	59.67	24.06	3.97	10.89	2.24	2.35
Standard deviation	46.58	9.77	1.09	5.36	0.29	0.24

Table 9 Statistics of the testing data for the results of the saturated samples

Statistical measure	UCS (MPa)	RL	V_p	η	ρ_d	ρ_{sat}
Minimum	10.40	2.59	8.48	1.83	1.98	2.59
Maximum	108.56	4.89	19.09	2.42	2.51	4.89
Mean	50.70	3.70	12.91	2.11	2.24	3.70
Standard deviation	49.05	1.04	4.12	0.28	0.24	1.04

to cover training and testing datasets. The statistics of these datasets are listed in Tables 8 and 9. In addition, similar to the dry case five hybrid models have been developed, where:

- Hybrid model 6 correlates the UCS (for the saturated samples) with the RL and V_p.
- Hybrid model 7 establishes a relationship between the UCS (for the saturated samples) with the RL, V_p, and ρ_d.
- Hybrid model 8 uses the variables RL, V_p, and ρ_{sat} to estimate the UCS (for the saturated samples).
- Hybrid model 9 observes the accuracy of predicting the UCS (for the saturated samples) using the RL, V_p, and η.
- Hybrid model 10 provides a relationship between the UCS (for the saturated samples) with the RL, V_p, η, ρ_d and ρ_{sat}.

The developed models for the saturated case are presented in Table 10. Section 4.3 reports the results of the verification of these models.

4.3 Verification of the Developed Models

The relationship of the obtained-measured UCS using the developed models and the correlation proposed by Mohammed et al. (2020) using the training and testing datasets are shown in Figs. 13a–f. It is clear from the figures that there is some scatter in the prediction of the developed models compared to the perfect fit line for some cases. However, the scatter of the developed models is lower than that produced using Mohammed et al. (2020) correlation. Figures 14a–c present the results of the statistical assessment for the developed models and the correlation of Mohammed et al. (2020). Figure 14a indicates that the produced MAE for the testing data is lower than that for the training data, which is due to the use of limited range for the testing data compared to the training data. Also, all of the new models scored MAE lower than that scored using Mohammed et al. (2020) correlation for the training data group.

Figure 14b indicates that all of the models scored mean close to 1.0 and with the same range for both training and testing data (1.02–1.09 for training data and 1.00–1.16 for testing data). This also provides additional confidence in the ability of the developed models to predict the testing data. The figure also shows that the new models produce mean better than Mohammed et al. (2020) correlation for the case of training data. Figure 14c shows that there is no significant difference in the obtained R for the developed models despite the difference in the number of variables employed in the development of the models for both training and testing groups. Furthermore, all of the new models scored better R than Mohammed et al. (2020) correlation. However, it is worthy to mention that Mohammed et al. (2020) correlation performed well considering that it only uses the Schmidt hammer to predict the UCS.

Finally, Fig. 15 provides much better insight regarding the performance by comparing the cumulative frequency and the error level for new models (6–10) and Mohammed et al. (2020) correlation. The figure shows that Mohammed et al. (2020) correlation provides the same error level as for hybrid models 6, 8 and 9 and outperform these models when the level of error becomes more than 40%. However, model 7 provides lower error with higher frequency compared to all other models for error range between 0 and 44%. Model 10, however, provides the highest frequency beyond error level of 44%.

Table 10 The hybrid models developed using the results of the saturated samples

Correlation name	Mathematical formulation	Parameters employed in development of the hybrid model
Hybrid model 6	$UCS = -409.43 \times \sqrt{V_p} + 114.9 \times \sqrt{RL} \times V_p - 3.85 \times V_p^2 \times RL - 0.338 \times RL^2 \times V_p + 0.1 \times RL^2 \times V_p^2 - 31.9$	Schmidt hummer rebound and ultrasonic
Hybrid model 7	$UCS = \frac{384010.4}{RL^2 \times V_p^2} - \frac{11803.34}{\sqrt{RL} \times \sqrt{V_p}} - 1.36 \times RL \times V_p^2 \times \sqrt{\rho_d} - 0.81 \times \frac{RL^2 \times V_p}{\rho_d} + 0.15 \frac{RL^2 \times V_p^2}{\sqrt{\rho_d}} + 1931.83$	Schmidt hummer rebound, ultrasonic and dry density
Hybrid model 8	$UCS = 53.83 \times \sqrt{RL} \times \sqrt{\rho_{sat}} \times V_p - 8.95 \times \sqrt{RL} \times \sqrt{\rho_{sat}} \times V_p^2 - 0.2 \times RL^2 \times \rho_{sat} \times \sqrt{V_p} + 0.03 \times \sqrt{\rho_{sat}} \times RL^2 \times V_p^2 - 333.3$	Schmidt hummer rebound, ultrasonic and saturated density
Hybrid model 9	$UCS = 47.7 \times \sqrt{V_p} + 1.9 \times \sqrt{RL} \times V_p \times \eta - 0.026 \sqrt{RL} \times V_p^2 \times \eta^2 - 0.053 \times RL^2 \times V_p + 0.0099 \times V_p^2 \times RL^2 - 165.25$	Schmidt hummer rebound, ultrasonic and porosity
Hybrid model 10	$UCS = 0.04 \times \sqrt{RL \times V_p^2 \times \eta \times \rho_d^2 \times \rho_{sat}} + 2.1 \times RL \times \sqrt{V_p \times \eta \times \gamma_d \times \rho_{sat}} - 0.5 \times RL \times V_p \times \sqrt{\eta \times \rho_{sat}^2} - 0.00075 \times RL \times V_p^2 \times \mu^2 \times \rho_d \times \rho_{sat} + 0.0026 \times RL^2 \times V_p^2 \times \sqrt{\rho_d \times \rho_{sat}} - 96.8$	Schmidt hummer rebound, ultrasonic, porosity, saturated density, and dry density

To sum up, it is clear that despite that the new models scored better statistical performance compared to Mohammed et al. (2020) correlation, some of these models did not show any enhanced predictions when compared using the cumulative frequency of the level of error. However, models 7 and 10 showed enhanced predictions and hence, these models could be suggested in future to achieve better accuracy than the available correlations in the literature.

5 The Usefulness of the Models in Practice

It is well known from the literature that the destructive tests (DT) are much more expensive than non-destructive tests (NDT) in terms of the required time to do the tests and the associated costs (Aboutaleb et al. 2018). Hence, this factor was one of the main motivations to do this research. In addition, it is not always feasible to obtain intact samples with length to diameter ratio of 2.0–2.5 as per the ASTM D7012-14e1 (2014). Thus, the models proposed in this study would be of significant help in practice when intact samples cannot be obtained with the desired length to diameter ratio. Also, Hybrid models 1 and 6 require only the NDT tests (Schmidt hammer and ultrasonic pulse velocity) and hence, these models could be used in prediction if the budget is limited as the direct testing of the UCS (destructive test) requires a calibrated compression testing machine which is expensive and not always available in geotechnical laboratories. Also, the other variables (dry density, saturated density, and porosity) require simple efforts and cheap equipment. In addition, the provided models could also be used as an independent quality control check on the results of laboratory tests.

6 Conclusions

Specimens of limestone rocks have been collected from north of Iraq (Mosul and Sulaymaniyah Provinces) and subjected to an extensive laboratory program to find the relationship of the unconfined compressive strength (UCS) with the Schmidt hummer rebound number, ultrasonic pulse velocity, porosity, dry density, and saturated density. In addition, the obtained results have been fed to an EPR-MOGA algorithm to propose new and more accurate soft computing-based models to facilitate more accurate prediction of the UCS. The followings can be summarized based on the findings of this paper:

1. Results of experimental program showed a general trend for the UCS to increase as the Schmidt hummer rebound number, ultrasonic pulse velocity, dry unit weight and saturated unit weight increases. However, the UCS is

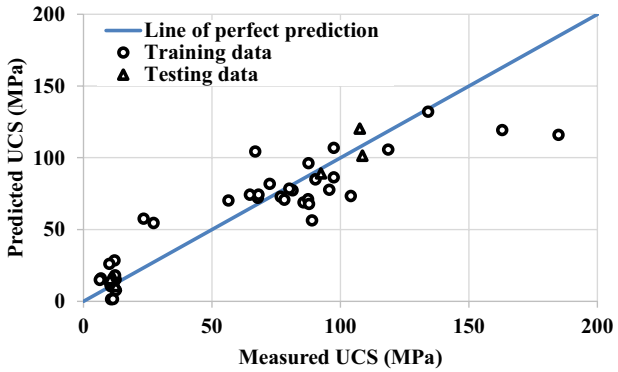

(a) Hybrid model 6

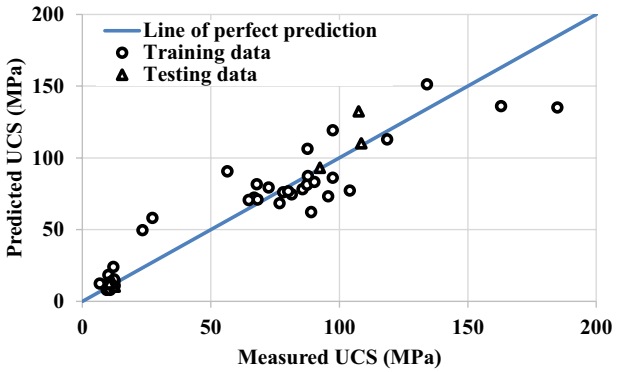

(b) Hybrid model 7

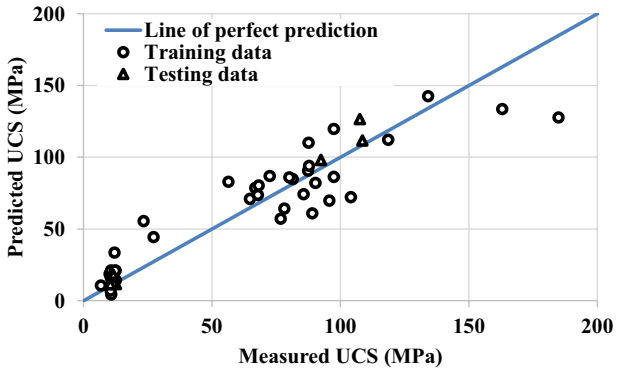

(c) Hybrid model 8

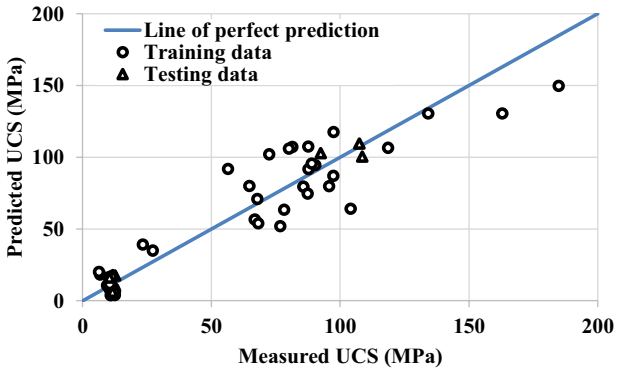

(d) Hybrid model 9

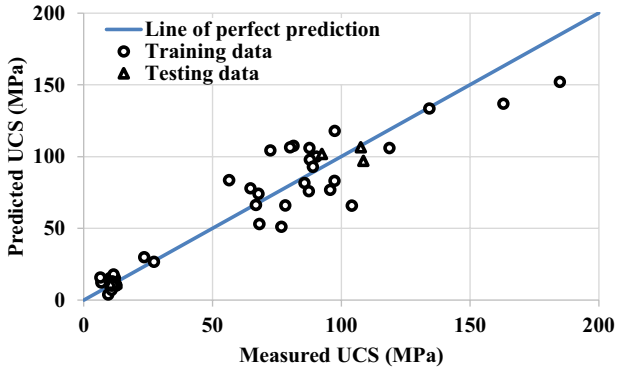

(e) Hybrid model 10

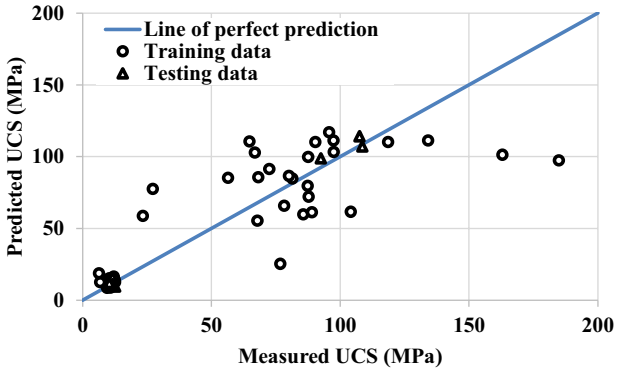

(f) Mohammed et al. (2020)

Fig. 13 Comparison of the relationship of the obtained–measured UCS with the line of perfect fit for the case of saturated samples for the proposed models and the correlation of Mohammed et al. (2020)

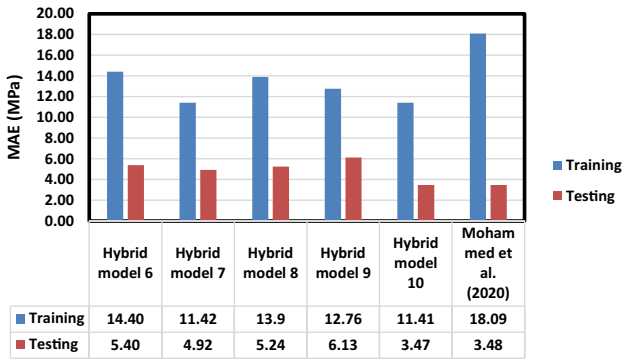

	Hybrid model 6	Hybrid model 7	Hybrid model 8	Hybrid model 9	Hybrid model 10	Mohammed et al. (2020)
Training	14.40	11.42	13.9	12.76	11.41	18.09
Testing	5.40	4.92	5.24	6.13	3.47	3.48

(a) Mean absolute error

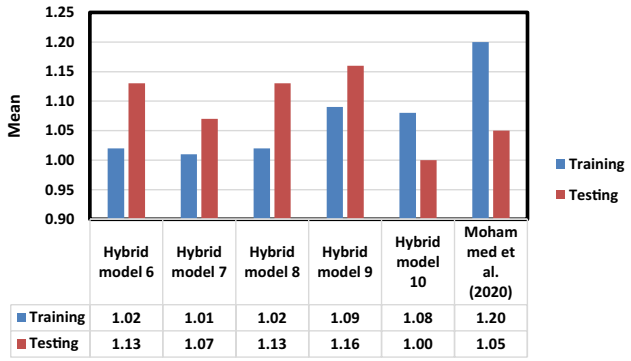

	Hybrid model 6	Hybrid model 7	Hybrid model 8	Hybrid model 9	Hybrid model 10	Mohammed et al. (2020)
Training	1.02	1.01	1.02	1.09	1.08	1.20
Testing	1.13	1.07	1.13	1.16	1.00	1.05

(b) Mean

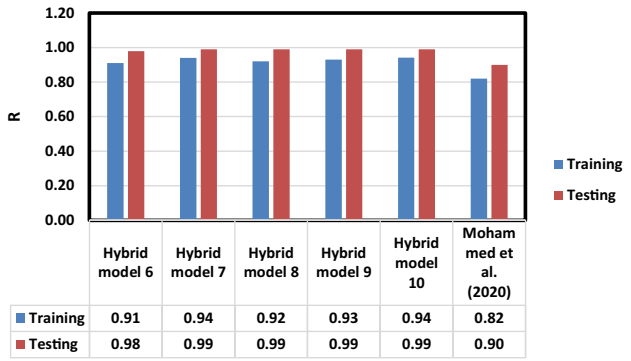

	Hybrid model 6	Hybrid model 7	Hybrid model 8	Hybrid model 9	Hybrid model 10	Mohammed et al. (2020)
Training	0.91	0.94	0.92	0.93	0.94	0.82
Testing	0.98	0.99	0.99	0.99	0.99	0.90

(c) Coefficient of correlation

Fig. 14 Statistical performance of the new hybrid models and Mohammed et al. (2020) correlation

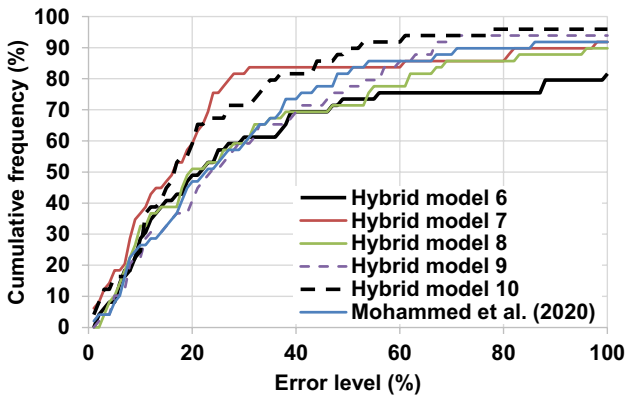

Fig. 15 Relationship between the cumulative frequency and the error level for hybrid models 6–10 and Mohammed et al. (2020) correlation

found to generally decrease as the porosity of the rock rises.

2. Bilinear relationships between the UCS and Schmidt hummer rebound number, ultrasonic pulse velocity, porosity, dry unit weight and saturated unit weight are found to provide average prediction for the UCS with R ranges between 0.69 and 0.88. Thus, the UCS cannot be predicted with excellent accuracy using only a bilinear relationship.
3. 10 new models have been proposed to predict the UCS in dry and saturated conditions. The models use combination of two, three, four and five variables; these variables are Schmidt hummer rebound number, ultrasonic pulse velocity, porosity, dry unit weight and saturated unit weight.
4. The accuracy of the developed models has been examined against a recent correlation proposed for limestone rocks by Mohammed et al. (2020). All of the models proposed for the dry condition outperformed the correlation of Mohammed et al. (2020), and two of the models proposed for the saturated condition outperformed the aforementioned recent correlation.
5. The new models enhance the accuracy of the prediction and uses only results of non-destructive testing. Thus, these models help rock engineers to optimize predictions and, hence, provide worthy addition to the state of the art on the topic. The models could also be utilized to conduct a verification check on the results of the UCS provided from the laboratory.

Appendix 1

See Tables 11 and 12.

Table 11 Results of the tests on dry rock samples

Schmidt hammer rebound number (RL)	Ultrasonic pulse velocity (V_p), (km/s)	Porosity (η), (%)	Dry density (g/cm^3)	Saturated density (g/cm^3)	Unconfined compressive strength (MPa)
36.55	4.38	9.920814	2.387	2.486	117.72
35.43	4.77	8.578812	2.411	2.497	119.59
36.98	4.94	6.94562	2.413	2.482	177.96
37.24	4.76	8.617303	2.399	2.485	156.55
40.42	4.54	10.11339	2.372	2.473	137.75
43.35	4.82	9.475679	2.394	2.489	128.39
36.21	4.95	9.149205	2.396	2.487	144.79
38.36	4.89	8.816329	2.381	2.469	98.98
36.47	5.04	8.062225	2.429	2.510	174.93
37.41	4.94	7.685354	2.401	2.478	86.78
30.10	4.79	8.170841	2.359	2.440	118.29
34.23	5.23	5.5232	2.495	2.550	181.64
32.08	4.54	8.985911	2.373	2.463	91.63
28.12	3.22	13.59443	2.276	2.412	62.89
31.48	3.99	9.930157	2.360	2.459	83.75
29.41	4.43	10.20099	2.257	2.359	92.98
33.97	5.01	6.491651	2.492	2.557	182.15
33.20	4.67	8.885364	2.417	2.506	121.52
27.09	3.55	6.469559	2.394	2.459	103.14
33.28	3.45	11.1357	2.060	2.171	51.44
29.41	4.95	9.680736	2.108	2.205	61.78
27.01	3.70	13.53067	2.425	2.561	75.74
29.50	3.70	3.545846	2.510	2.545	24.45
35.61	5.22	2.772497	2.537	2.565	38.67
33.97	5.83	1.752549	2.619	2.637	46.97
31.65	3.86	9.401795	2.397	2.491	61.85
30.62	4.82	7.090966	2.487	2.558	126.76
35.43	5.08	4.415805	2.475	2.519	42.46
31.39	5.59	2.481633	2.668	2.693	68.63
31.31	4.88	6.409257	2.510	2.574	125.74
26.49	5.66	1.511486	2.606	2.621	34.75
31.99	4.82	7.125606	2.479	2.550	121.22
36.04	5.17	3.928184	2.564	2.604	105.57
18.66	2.85	19.79642	1.911	2.109	21.187
19.01	2.91	18.44559	1.958	2.143	23.880
19.78	2.90	19.0575	1.996	2.186	26.080
18.58	2.75	18.38358	1.882	2.065	22.607
17.72	2.77	19.02159	2.066	2.256	29.128
18.58	2.90	19.31154	2.060	2.253	27.845
17.46	2.69	20.00258	2.042	2.242	27.600
19.52	2.78	20.0881	1.922	2.123	20.938
18.23	2.99	18.40507	2.056	2.240	28.250
17.55	2.98	18.35052	2.038	2.221	30.681
20.21	2.88	18.62168	2.049	2.235	26.786
20.73	2.80	20.5959	2.039	2.245	28.082
16.26	3.02	16.66905	1.904	2.070	16.977
15.48	2.98	17.12931	1.864	2.035	16.045
16.17	3.01	16.59257	1.879	2.045	18.427

Table 11 (continued)

Schmidt hammer rebound number (RL)	Ultrasonic pulse velocity (V_p), (km/s)	Porosity (η), (%)	Dry density (g/cm^3)	Saturated density (g/cm^3)	Unconfined compressive strength (MPa)
13.59	3.03	16.74469	1.880	2.047	17.804
15.22	2.93	18.58988	1.838	2.024	13.740
15.05	2.86	19.12331	1.803	1.994	12.969
17.37	2.88	17.5735	1.797	1.973	15.483
15.40	2.90	18.06353	1.809	1.990	13.806

Table 12 Results of the tests on saturated rock samples

Schmidt hammer rebound number (RL)	Ultrasonic pulse velocity (V_p), (km/s)	Porosity (η), (%)	Dry density (g/cm^3)	Saturated density (g/cm^3)	Unconfined compressive strength (MPa)
35.61	4.53	8.262	2.415	2.498	90.34
36.72	4.42	9.814	2.375	2.473	95.72
33.63	4.74	8.475	2.423	2.508	92.46
35.61	4.79	8.585	2.412	2.498	118.66
35.69	4.40	9.748	2.371	2.468	64.76
35.78	4.54	9.542	2.385	2.480	97.43
35.09	4.79	9.147	2.395	2.486	108.56
36.29	4.89	8.853	2.412	2.500	107.51
35.78	5.09	7.589	2.443	2.519	134.19
34.40	4.97	8.112	2.432	2.513	97.49
29.93	4.54	10.333	2.288	2.392	87.44
34.06	5.29	5.187	2.497	2.549	162.96
33.80	4.87	8.664	2.413	2.499	87.64
16.34	4.00	7.899	2.425	2.504	76.79
27.01	3.98	7.503	2.441	2.516	78.26
25.63	4.47	9.323	2.330	2.424	85.72
33.37	5.54	5.267	2.535	2.588	184.87
24.60	4.35	9.993	2.313	2.413	67.89
26.06	4.15	6.678	2.417	2.484	104.13
25.97	4.86	6.394	2.422	2.486	89.02
28.38	4.68	6.567	2.241	2.307	87.79
25.37	4.80	3.234	2.519	2.551	23.47
33.03	5.10	3.578	2.485	2.521	38.63
31.13	5.70	1.619	2.613	2.629	68.19
29.50	3.71	13.314	2.275	2.408	27.32
31.31	4.82	6.922	2.487	2.557	80.13
32.34	5.31	2.973	2.518	2.548	35.69
31.05	5.80	2.321	2.560	2.583	56.47
32.25	4.74	6.856	2.483	2.551	72.51
30.96	4.89	6.528	2.501	2.566	81.46
34.32	4.93	3.259	2.690	2.723	66.89
12.30	2.76	18.306	1.966	2.149	12.54
12.04	2.68	18.146	1.940	2.121	12.65
13.25	2.59	19.092	1.939	2.130	11.64
12.99	2.56	18.927	1.973	2.162	10.64
11.95	2.51	17.727	2.068	2.245	11.13

Table 12 (continued)

Schmidt hammer rebound number (RL)	Ultrasonic pulse velocity (V_p), (km/s)	Porosity (η), (%)	Dry density (g/cm^3)	Saturated density (g/cm^3)	Unconfined compressive strength (MPa)
11.61	2.48	17.669	2.055	2.231	10.58
12.81	2.60	19.269	1.918	2.111	10.96
12.81	2.70	18.530	1.944	2.129	12.39
12.64	2.60	17.510	2.066	2.241	10.74
13.42	2.78	17.888	2.050	2.229	12.10
12.90	2.41	17.133	2.084	2.256	11.56
14.19	2.44	12.246	1.367	1.490	6.45
12.90	2.84	16.318	1.822	1.985	10.15
11.52	2.96	14.879	1.872	2.021	11.73
10.66	2.95	15.932	1.865	2.025	10.82
10.92	3.07	14.312	1.924	2.067	12.62
12.56	3.10	14.567	1.911	2.056	12.45
11.87	2.87	15.645	1.828	1.984	10.40
12.04	2.83	15.408	1.812	1.966	6.80
10.58	2.81	16.140	1.789	1.950	9.54

Author contributions SA: conceptualization, methodology, validation, formal analysis, writing—original draft. DAM: data, experimental testing, methodology, writing—review and editing. YMA: methodology, Writing—review and editing.

Funding No funding was received for conducting this study.

Availability of data and materials Data used in this research are available upon request.

Code availability Code used in this research is available upon request.

Declarations

Conflict of interest/Competing interests The authors declare no conflict of interest associated with this submission. In addition, the authors have no relevant financial or non-financial interests to disclose.

References

Deer DU, Miller R (1966) Engineering classification and index properties for intact rock. Deformation Curve AFNL-TR, 65–116.

Aboutaleb S, Behnia M, Bagherpour R, Bluekian B (2018) Using non-destructive tests for estimating uniaxial compressive strength and static Young's modulus of carbonate rocks via some modeling techniques. Bull Eng Geol Environ 77(4):1717–1728

Ahangar-Asr A, Javadi AA, Johari A, Chen Y (2014) Lateral load bearing capacity modelling of piles in cohesive soils in undrained conditions: an intelligent evolutionary approach. Appl Soft Comput 24:822–828

Alzabeebee S (2019) Seismic response and design of buried concrete pipes subjected to soil loads. Tunn Undergr Space Technol 93:103084

Alzabeebee S (2020) Application of EPR-MOGA in computing the liquefaction-induced settlement of a building subjected to seismic shake. Eng Comput. https://doi.org/10.1007/s00366-020-01159-9

Alzabeebee S, Chapman DN (2020) Evolutionary computing to determine the skin friction capacity of piles embedded in clay and evaluation of the available analytical methods. Transport Geotech 24:100372

Alzabeebee S, Alshkane YM, Rashed KA (2021a) Evolutionary computing of the compression index of fine-grained soils. Arab J Geosci 14(19):1–17. https://doi.org/10.1007/s12517-021-08319-1

Alzabeebee S, Alshkane YM, Al-Taie AJ, Rashed KA (2021b) Soft computing of the recompression index of fine-grained soils. Soft Comput. https://doi.org/10.1007/s00500-021-06123-3

ASTM D7012-14e1 (2014) Standard Test Method for Compressive Strength and Elastic Moduli of Intact Rock Core Specimens under Varying States of Stress and Temperatures. ASTM International, West Conshohocken, PA.

Azimian A (2017) Application of statistical methods for predicting uniaxial compressive strength of limestone rocks using nondestructive tests. Acta Geotech 12(2):321–333

Aziz BK, Baban EN (2005) Resistivity properties of limestone rocks in parts of Iraqi Kurdistan Region-NE Iraq. J Zankoy Sulaimani 8(1):257–267

Barone G, Mazzoleni P, Pappalardo G, Raneri S (2015) Microtextural and microstructural influence on the changes of physical and mechanical proprieties related to salts crystallization weathering in natural building stones. The example of Sabucina stone (Sicily). Constr Build Mater 95:355–365. https://doi.org/10.1016/j.conbuildmat.2015.07.131

Baykasoğlu A, Güllü H, Çanakçı H, Özbakır L (2008) Prediction of compressive and tensile strength of limestone via genetic programming. Expert Syst Appl 35(1–2):111–123

Beiki M, Majdi A, Givshad AD (2013) Application of genetic programming to predict the uniaxial compressive strength and elastic modulus of carbonate rocks. Int J Rock Mech Min Sci 1997(63):159–169

Cargill JS, Shakoor A (1990) Evaluation of empirical methods for measuring the uniaxial compressive strength of rock. Int J Rock Mech Min Sci Geomech Abstr 27(6):495–503

Cherblanc F, Berthonneau J, Bromblet P, Huon V (2016) Influence of water content on the mechanical behaviour of limestone: Role of the clay minerals content. Rock Mech Rock Eng 49(6):2033–2042

Çobanoglu İ, Celik SB (2008) Estimation of uniaxial compressive strength from point load strength, Schmidt hardness and P-wave velocity. Bull Eng Geol Environ 67(4):491–498

Daoud HSD, Rashed KAR, Alshkane YMA (2017) Correlations of uniaxial compressive strength and modulus of elasticity with point load strength index, pulse velocity and dry density of limestone and sandstone rocks in Sulaimani Governorate, Kurdistan Region, Iraq. J Zankoy Sulaimani-Part A-(pure and Applied Sciences) 19:57–72. https://doi.org/10.17656/jzs.10632

Daoud HS, Alshkane YM, Rashed KA (2018) Prediction of uniaxial compressive strength and modulus of elasticity for some sedimentary rocks in Kurdistan Region-Iraq using Schmidt Hammer. Kirkuk Univ J Sci Stud 13(1):52–67

Ebdali M, Khorasani E, Salehin S (2020) A comparative study of various hybrid neural networks and regression analysis to predict unconfined compressive strength of travertine. Innov Infrastruct Solut 5(3):1–14

Feng X, Jimenez R (2014) Bayesian prediction of elastic modulus of intact rocks using their uniaxial compressive strength. Eng Geol 173:32–40

Giustolisi O, Savic DA (2006) A symbolic data-driven technique based on evolutionary polynomial regression. J Hydroinf 8(3):207–222

Giustolisi O, Savic DA (2009) Advances in data-driven analyses and modelling using EPR-MOGA. J Hydroinf 11(3–4):225–236

Google.Map (2021) The location of the study area. Retrieved from https://www.google.com/maps/@33.8051178,46.9294439,6z?hl=en. Accessed 1 Sept 2021

Hebib R, Belhai D, Alloul B (2017) Estimation of uniaxial compressive strength of North Algeria sedimentary rocks using density, porosity, and Schmidt hardness. Arab J Geosci 10(17):1–13

ISRM (1981) Rock Characterization, testing and monitoring. ISRM suggested methods. Pergamon Press, Oxford

Jabbar MA (2011) Correlations of point load index and pulse velocity with the uniaxial compressive strength for rocks. J Eng 14:992–1006

Kahraman S (2001) Evaluation of simple methods for assessing the uniaxial compressive strength of rock. Int J Rock Mech Min Sci 38(7):981–994

Katz O, Reches Z, Roegiers JC (2000) Evaluation of mechanical rock properties using a Schmidt Hammer. Int J Rock Mech Min Sci 37(4):723–728

Kong F, Shang J (2018) A validation study for the estimation of uniaxial compressive strength based on index tests. Rock Mech Rock Eng 51(7):2289–2297

Kurtuluş C, Sertçelik FADİME, Sertçelik I (2016) Correlating physico-mechanical properties of intact rocks with P-wave velocity. Acta Geod Geoph 51(3):571–582. https://doi.org/10.1007/s40328-015-0145-1

Mahmoodzadeh A, Mohammadi M, Ali HFH, Abdulhamid SN, Ibrahim HH, Noori KMG (2021) Dynamic prediction models of rock quality designation in tunneling projects. Transport Geotech 27:100497

Mahmoodzadeh A, Mohammadi M, Ghafoor Salim S, Farid Hama Ali H, Hashim Ibrahim H, Nariman Abdulhamid S, Nejati HR, Rashidi S (2022) Machine learning techniques to predict rock strength parameters. Rock Mech Rock Eng. https://doi.org/10.1007/s00603-021-02747-x

Miah MI, Ahmed S, Zendehboudi S, Butt S (2020) Machine learning approach to model rock strength: prediction and variable selection with aid of log data. Rock Mech Rock Eng 53(10):4691–4715

Minaeian B, Ahangari K (2013) Estimation of uniaxial compressive strength based on P-wave and Schmidt hammer rebound using statistical method. Arab J Geosci 6(6):1925–1931

Mirza TA, Mohialdeen IM, Al-Hakarri SH, Fatah CM (2016) Geochemical assessment of Naopurdan limestone for cement making-Chwarta area, Kurdistan Region, NE Iraq. J ZANKOY SULAIMANI Spec Issue GeoKurdistan II:257–267

Mishra DA, Basu A (2013) Estimation of uniaxial compressive strength of rock materials by index tests using regression analysis and fuzzy inference system. Eng Geol 160:54–68. https://doi.org/10.1016/j.enggeo.2013.04.004

Mohammed DA, Alshkane YM, Hamaamin YA (2020) Reliability of empirical equations to predict uniaxial compressive strength of rocks using Schmidt hammer. Georisk 14(4):308–319

Momeni E, Armaghani DJ, Hajihassani M, Amin MFM (2015) Prediction of uniaxial compressive strength of rock samples using hybrid particle swarm optimization-based artificial neural networks. Measurement 60:50–63

Monjezi M, Khoshalan HA, Razifard M (2012) A neuro-genetic network for predicting uniaxial compressive strength of rocks. Geotech Geol Eng 30(4):1053–1062

Numan NMS, Hammoudi RA, Chorowicz J (1998) Synsedimentary tectonics in the Eocene Pila Spi limestone formation in Iraq and its geodynamic implications. J Afr Earth Sci 27(1):141–148

Ozer M, Isik NS, Orhan M (2008) Statistical and neural network assessment of the compression index of clay-bearing soils. Bull Eng Geol Environ 67(4):537–545

Sabatakakis N, Koukis G, Tsiambaos G, Papanakli S (2008) Index properties and strength variation controlled by microstructure for sedimentary rocks. Eng Geol 97(1–2):80–90

Sachpazis CI (2004) Monitoring degree of metamorphism in a four-stage alteration process passing from pure limestone to pure marble. Electron J Geotech Eng, p 416

Shahnazari H, Tutunchian MA (2012) Prediction of ultimate bearing capacity of shallow foundations on cohesionless soils: an evolutionary approach. KSCE J Civ Eng 16(6):950–957

Singh TN, Kainthola A, Venkatesh A (2012) Correlation between point load index and uniaxial compressive strength for different rock types. Rock Mech Rock Eng 45(2):259–264

Sissakian V, Ghafur AA, Omer S, Khalil D (2021) Industrial assessment of limestone beds of the Qamchuqa formation for cement industry, Kurdistan Region, North Iraq. UKH J Sci Eng 5(2):62–71

Vásárhelyi B (2005) Statistical analysis of the influence of water content on the strength of the Miocene limestone. Rock Mech Rock Eng 38(1):69–76

Wang M, Wan W (2019) A new empirical formula for evaluating uniaxial compressive strength using the Schmidt hammer test. Int J Rock Mech Min Sci 123:104094

Yurdakul M, Akdas H (2013) Modeling uniaxial compressive strength of building stones using non-destructive test results as neural networks input parameters. Constr Build Mater 47:1010–1019

Zhang W, Goh AT (2016) Multivariate adaptive regression splines and neural network correlations for prediction of pile drivability. Geosci Front 7(1):45–52

Zhang W, Zhang R, Wu C, Goh ATC, Lacasse S, Liu Z, Liu H (2020) State-of-the-art review of soft computing applications in underground excavations. Geosci Front 11(4):1095–1106

Publisher's Note Springer Nature remains neutral with regard to jurisdictional claims in published maps and institutional affiliations.